Available online at www.sciencedirect.com
ScienceDirect
Applied Mathematical Modelling 31 (2007) 1124–1132
APPLIED MATHEMATICAL MODELLING
www.elsevier.com/locate/apm

Modeling and simulation of plasma jet by lattice Boltzmann method

Haiou Zhang, Shengde Hu *, Guilan Wang, Jieying Zhu

State Key Lab of Plastic Forming Simulation and Die and Mold Tech., Huazhong University of Science and Technology, Wuhan 430074, China

Received 1 September 2005; received in revised form 1 November 2005; accepted 16 March 2006
Available online 12 June 2006

Abstract

In order to find a simple and efficient simulation for plasma spray process, an attempt of modeling was made to calculate velocity and temperature field of the plasma jet by hexagonal 7-bit lattice Boltzmann method (LBM) in this paper. Utilizing the methods of Chapman–Enskog expansion and multi-scale expansion, the authors derived the macro equations of the plasma jet from the lattice Boltzmann evolution equations on the basis of selecting two opportune equilibrium distribution functions. The present model proved to be valid when the predictions of the current model were compared with both experimental and previous model results. It is found that the LBM is simpler and more efficient than the finite difference method (FDM). There is no big variation of the flow characteristics, and the isotherm distribution of the turbulent plasma jet is compared with the changed quantity of the inlet velocity. Compared with the velocity at the inlet, the temperature at the inlet has a less influence on the characteristics of plasma jet.

Keywords: Plasma jet; Simulation and modeling; Lattice Boltzmann method

1. Introduction

Plasma jets are widely used for corrosion-, heat-, and abrasion-resistant coatings of monolithic and near-net shapes of metallic and ceramic parts [1,2]. Nowadays, plasma jets have also been applied to the field of rapid tooling (RT) and waste treatment [3]. As the state of plasma jet influences the velocity, the temperature and the melt fraction of the sprayed powder particles, it can affect the quality and formability of thermal spray coatings. Because of high temperature (up to 10^4 K), high flow velocity (up to several hundred meters per second) and great gradients in plasma jets, it is not easy to exactly diagnose the characteristics of plasma jets. A theoretical modeling is an important tool to improve the understanding of the plasma process. Many researchers have carried out modeling and simulation of the plasma jet by SIMPLE algorithm, or compute fluid dynamics (CFD) software such as LAVA, FLUENT, and PHOENICS [4–7]. These well-established models

* Corresponding author. Tel.: +86 27 87543493; fax: +86 27 87544071/87557394.
E-mail addresses: adhello@163.com, zholab@mail.hust.edu.cn (S. Hu).

0307-904X/$ - see front matter
doi:10.1016/j.apm.2006.03.028

are extraordinarily helpful to improve the understanding of the physical nature of the plasma jet, the relationship between the key process parameters and the effective control of the coating quality. However, to the authors' knowledge, the reported models are mainly at the macroscopic level and are based on the finite difference method (FDM) or the finite element method (FEM). Generally, in these models the SIMPLE (or SIMPLER, SIMPLEST) algorithm and stagger grids are often used to solve the large equations set, where the unsuitable pressure must be eliminated. As a result, the program becomes complex and the simulation speed is slow. In order to find a simple and efficient calculation for the plasma spray process, an attempt of simulating the plasma jet by the lattice Boltzmann method (LBM) at the microscopic level is made in this paper.

Lattice Boltzmann was put forward with real variables in 1988 [8,9], which is developed from Boolean Lattice Gas Automata. The single relaxed lattice BGK [10] simplifies LB equation and has more flexibility and efficiency. Since then the LBM has been widely used for modeling physical systems [11] and solving partial differential equations, especially in CFD [12]. Unlike conventional numerical schemes based on discretization of macroscopic continuum equations, LBM constructs simplified kinetic models that incorporate the essential physics of microscopic or mesoscopic processes so that the average properties obey the desired macroscopic partial differential equation. The special character of lattice Boltzmann method is its simple idea and instinctive physical picture. It also provides easily implemented, fully parallel algorithms and the capability of handling complicated bounds.

2. Numerical model

2.1. LB evolution equation for plasma jet

The basic assumption of calculation is that the jet is in a local thermodynamic equilibrium state and is optically thin. The calculation domain is the section parallel to the axis shown in Fig. 1. It shows a calculating model of grid division. It consists of hexagonal 7-bit lattices. The velocity vector of grid is expressed as

$$\vec{c}_i = \begin{cases} C(\cos a_i, \sin a_i); & i = 1, \ldots, 6 \\ 0; & i = 0, \end{cases} \quad \text{where } a_i = \mathrm{pi}(2i-1)/6, \text{ and } C \text{ is velocity of grid.}$$

A multi-speed lattice Boltzmann model is usually chosen for calculating the temperature change of the thermal flow, in which different speeds represent different energies [9]. The model, however, is not appropriate for simulating the heat and velocity field of the plasma jet because of the existence of great temperature and velocity gradient. In this paper, two sets of lattice Boltzmann equations with BGK collision operator are chosen in the following form:

$$\begin{aligned} f_i(\vec{x} + \vec{c}_i\varepsilon, t+\varepsilon) - f_i(\vec{x}, t) &= -\frac{1}{\tau}\left[f_i(\vec{x}, t) - f_i^{(0)}(\vec{x}, t)\right], \\ T_i(\vec{x} + \vec{c}_i\varepsilon, t+\varepsilon) - T_i(\vec{x}, t) &= -\frac{1}{\tau_T}\left[T_i(\vec{x}, t) - T_i^{(0)}(\vec{x}, t)\right] - \frac{\dot{q}\alpha_i}{\rho C_p}, \end{aligned} \tag{1}$$

where i and α_i are the direction number particles moving and percent of the i direction particles; f_i and T_i are distribution of density and temperature, respectively; $f_i^{(0)}$ and $T_i^{(0)}$ are the local equilibrium distribution of f_i

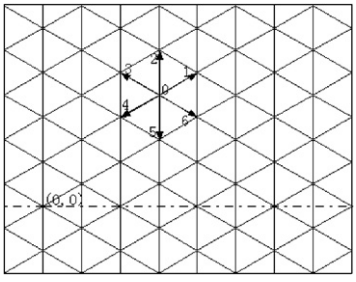

Fig. 1. Lattice grid model of fluid field.

and T_i; τ and τ_T are relaxation factors; $\vec{x}$, $\vec{c}_i$ and ε are position vector, velocity vector and time step which has a minimal value; and $\dot{q}$ is the radiance per unit volume of plasma jet. The key to generating the correct macroscopic hydrodynamic equations is in the choice of the equilibrium distribution functions $f_i^{(0)}$ and $T_i^{(0)}$ [12]. These have the form

$$f_i^{(0)} = A_0 - A_1 v^2 + A_2(\vec{c}_i \cdot \vec{v}) + A_3(\vec{c}_i \cdot \vec{v})^2, \qquad f_0^{(0)} = D_0 - D_1 v^2, \qquad T_i^{(0)} = B_0 + B_1(\vec{c}_i \cdot \vec{v}),$$
$$T_0^{(0)} = E_0 \quad (i = 1, 2, 3, 4, 5, 6). \tag{2}$$

To derive the macro equation of the plasma jet, the left items of Eq. (1) are expanded by Taylor series and, a multi-scale method (Eq. (3)), while the right items are expanded by the Chapman–Enskog method [13].

$$\left.\begin{aligned} f_i &= f_i^{(0)} + \varepsilon f_i^{(1)} + \varepsilon^2 f_i^{(2)} + \cdots, \qquad T_i = T_i^{(0)} + \varepsilon T_i^{(1)} + \varepsilon^2 T_i^{(2)} + \cdots \\ \frac{\partial}{\partial t} &= \frac{\partial}{\partial t_0} + \varepsilon \frac{\partial}{\partial t_1} + \varepsilon^2 \frac{\partial}{\partial t_2} \end{aligned}\right\}. \tag{3}$$

Substituting the above expansions into Eq. (1), equations of the first and second order in ε ψ are written as

$$\left(\frac{\partial}{\partial t_0} + c_i \nabla\right) f_i^{(0)} = -\frac{1}{\tau} f_i^{(1)}, \tag{4}$$

$$\frac{\partial f_i^{(0)}}{\partial t_1} + \left(\frac{\partial}{\partial t_0} + c_i \nabla\right)\left(1 - \frac{1}{2\tau}\right) f_i^{(1)} = -\frac{1}{\tau} f_i^{(2)}. \tag{5}$$

The mass and the momentum are conserved in collisions

$$\sum_i f_i = \sum_i f_i^{(0)} = \rho, \qquad \sum_i f_i^{(0)} c_{ik} = \rho v_{ik}. \tag{6}$$

When Eqs. (4) and (5) are summed over the i velocity, the mass conservation equation to second order is

$$\frac{\partial \rho}{\partial t} + \nabla(\rho v) = 0. \tag{7}$$

The momentum equation to the second order is obtained by multiplying the above equations by c_i and then summing over velocities,

$$\frac{\partial(\rho v)}{\partial t} + \nabla\left(\overset{(0)}{\prod} + \left(1 - \frac{1}{2\tau}\right)\overset{(1)}{\prod}\right) = 0, \tag{8}$$

where $\prod^{(0)}$ and $\prod^{(1)}$ are the momentum flux tensors, defined as

$$\overset{(0)}{\prod_{mn}} = \sum\nolimits_i f_i^{(0)} c_{im} c_{in} = p\delta_{mn} + \rho v_m v_n, \tag{9}$$

$$\overset{(1)}{\prod_{mn}} = \sum\nolimits_i f_i^{(1)} c_{im} c_{in}. \tag{10}$$

Substituting Eq. (2) into Eqs. (9) and (10) and using the velocity moment relations on the hexagonal 7-bit lattice, it is obtained that

$$\overset{(0)}{\prod_{mn}} = \frac{\rho c^2}{4}\delta_{mn} + \rho v_m v_n, \tag{11}$$

$$\overset{(1)}{\prod_{mn}} = (-\tau)\left[\frac{\partial}{\partial t_1}\overset{(0)}{\prod_{mn}} + \frac{\partial}{\partial x_\gamma}\sum_i f_i^{(0)} c_{im} c_{in} c_{i\gamma}\right] = (-\tau)\rho c_s^2\left(\frac{\partial v_n}{\partial x_m} + \frac{\partial v_m}{\partial x_n}\right)$$
$$= \frac{-\rho\tau}{2} S_{mn}, \tag{12}$$

where δ_{mn}, p and c_s are Kronecker delta, pressure ($p = \rho c_s^2$) and the local sound speed, respectively. Symbols m and n are coordinate quantities. The strain tensor S_{mn} is $\frac{1}{2}\left(\frac{\partial v_n}{\partial x_m} + \frac{\partial v_m}{\partial x_n}\right)$.

Using Eqs. (11) and (12) for Eq. (8), the final form of the momentum equation is as follows:

$$\frac{\partial \rho v}{\partial t} + \nabla \cdot \left(\rho \vec{v}\ \vec{v} + p\delta_{mn} \right) = \frac{\partial}{\partial x_n} \left[\mu_e \left[\frac{\partial v_m}{\partial x_n} + \frac{\partial v_n}{\partial x_m} \right] \right], \tag{13}$$

where μ_e is the effective viscosity, $\mu_e = (\tau - 0.5)\varepsilon\rho c_s^2 = (\tau - 0.5)\rho/4$.

Using a similar deducing process, the energy conservation equation and the temperature relaxation factor can also be acquired as follows:

$$\frac{\partial \rho T}{\partial t} + \nabla \cdot [\vec{v}(\rho T)] = \nabla \cdot [\Gamma_e \nabla T] - \dot{q}/C_p, \tag{14}$$

$$\tau_T = 0.5 + 2\Gamma_e/(\rho c^2 \varepsilon), \tag{15}$$

where $\Gamma_e = \Gamma + \Gamma_t = \lambda/C_p + \mu_t/Pr_t$, λ is thermal conductivity, C_p is specific heat and Pr_t is Prandtl number. The macro temperature of the plasma jet satisfies the following equation:

$$\sum_i T_i = T, \qquad \sum_i T_i c_{im} = T v_m. \tag{16}$$

In the deducing process, the coefficients of Eq. (2) are obtained as

$$A_0 = \rho/12, \quad A_1 = \rho/6, \quad A_2 = \rho/3, \quad A_3 = 2\rho/3, \quad D_0 = 0.5\rho, \quad D_1 = \rho, \quad B_0 = 0.15T,$$
$$B_1 = T/3, \quad E_0 = 0.1T.$$

2.2. LB subgrid turbulence model

A subgrid turbulence model for the lattice Boltzmann method is used here for consideration of the turbulent flow [14,15]. The subgrid turbulence modeling is achieved by incorporating the turbulence stress relation of a large-eddy simulation (LES) into the lattice Boltzmann method modeling [15–17]. In LES the contribution of the large, energy-carrying structures to momentum and energy transfer is computed exactly, and only the effect of the smallest scales of turbulence is modeled. In LES every physical quantity is divided into a large-scale quantity and a small-scale quantity [15]

$$\phi = \overline{\phi} + \phi', \tag{17}$$

where $\overline{\phi}$ is a large-scale quantity which is obtained by a space filtering operation,

$$\overline{\phi}(x,t) = \int \phi(x',t) K(x,x') \mathrm{d}x', \tag{18}$$

where K is a spatial filter function.

Applying the filtering operation for the Navier–Stokes equations (Eqs. (7) and (13)), we obtain

$$\left.\begin{aligned} &\nabla \bar{v} = 0 \\ &\tfrac{\partial \bar{v}}{\partial t} + \bar{v} \cdot \nabla \bar{v} = -\nabla \overline{P} + v \nabla^2 \bar{v} - \nabla R \end{aligned}\right\} \tag{19}$$

where v is kinematic viscosity, which equals $(\tau - 0.5)/4$; R_{mn} $(= \overline{v_m v_n} - \overline{v_m}\,\overline{v_n})$ is a subgrid stress tensor. According to Smagrinsky model, the anisotropic part of the subgrid stress tensor is modeled as

$$R_{mn} - \frac{1}{3} R_{\gamma\gamma} \delta_{mn} = -2 v_t \overline{S_{mn}} = -2 C_{\mathrm{smag}} \Delta^2 |\overline{S}| \overline{S_{mn}}, \tag{20}$$

where $\overline{S_{mn}}$ is a large-scale strain rate tensor, $\overline{S_{mn}} = \frac{1}{2}\left(\frac{\partial \overline{v_n}}{\partial x_m} + \frac{\partial \overline{v_m}}{\partial x_n} \right)$; $|\overline{S}| = (2 S_{mn} S_{mn})^{1/2}$; C_{smag} is the Smagorinsky constant; Δ is the width of the filtered function.

Assume that the total effective viscosity v_e consists of physical kinematic viscosity v_0 and the eddy viscosity term v_t, then

$$v_e = v_0 + v_t = v_0 + C_{\mathrm{smag}} \Delta^2 |\overline{S}| = (\tau_e - 0.5)/4. \tag{21}$$

According to Eq. (10) and non-equilibrium properties of the filtered particle distribution, non-equilibrium stress tensor, $\overline{\prod_{mn}^{\text{noneq}}}$, can be written as

$$\overline{\prod_{mn}^{\text{noneq}}} = \sum_i c_{im}c_{in}\left(\bar{f}_i - \overline{f_i^{(0)}}\right). \tag{22}$$

Considering the relation between stress and strain in Eq. (12), the magnitude of the large-scale strain rate tensor, $|\overline{S}|$, can be expressed as

$$|\overline{S}| = (2S_{mn}S_{mn})^{1/2} = 2\left(2\overline{\prod_{mn}^{\text{noneq}}}\,\overline{\prod_{mn}^{\text{noneq}}}\right)^{1/2} \Big/ \rho\tau_e. \tag{23}$$

Symbol τ_e is effective relax time. Utilizing Eqs. (21) and (23), $|\overline{S}|$ can be attained as the following:

$$|\overline{S}| = \frac{\sqrt{(4v_0+0.5)^2 + 32C_{\text{smag}}\Delta^2\rho^{-1}\left(2\overline{\prod_{mn}^{\text{noneq}}}\,\overline{\prod_{mn}^{\text{noneq}}}\right)^{1/2}} - (4v_0+0.5)}{8C_{\text{smag}}\Delta^2}. \tag{24}$$

In the simulations of the constant temperature flow by LBM, the diffusion coefficient is constant in evolution. But for the full length of the plasma jet, the temperature can vary up to ten thousand degrees and physical parameters such as v_0, λ, C_p and $\dot{q}$ are temperature-dependent. To make the calculation accurate, the discrete data in the literature [1] are fitted to the curves by Matlab. A proper grid length is also chosen to make the diffusion coefficient of LB fit for the real coefficient magnitude. To ensure that the computing is valid, the fluid must be subsonic for LB. As mentioned above, the atmospheric pressure plasma jet satisfies this because the temperature of Ar plasma jet is up to 10^4 K and its maximum velocity is under 1000 m/s.

2.3. Bound conditions

For the symmetry of the plasma jet, a half calculating region is plotted in Fig. 2. The left side OB is fixed bound expressed in Eq. (25). The left-up side BC adopts a non-slip rebound side; the central line OA is employed to symmetry side; the right side AD and the upper side CD are regarded as free bound.

$$v = v_0\left[1-(r/R)^2\right], \qquad T = (T_0 - T_w)\left[1-(r/R)^4\right] + T_w, \tag{25}$$

where v_0 and T_0 are maximum values of the plasma axial velocity and the temperature at exit, respectively, and T_w is the wall temperature of the gun.

2.4. Calculating process

1. Give the initial value of densities, temperatures and velocities of the whole field.
2. Calculate the magnitude of the large-scale strain rate tensor according to Eq. (24), the density relax factor and temperature relax factor according to Eqs. (15) and (21).

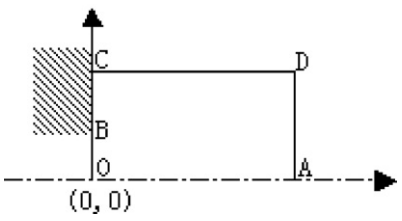

Fig. 2. The bound condition side.

3. Calculate the values of left bound according to Eq. (25), the inner equilibrium distributions of density and temperature according to Eq. (2). Calculate the inner distributions for the particle flight according to Eq. (1) and the distributions of bound.
4. Let the particles move a step, and record the flying-in distributions of density and temperature.
5. Calculate macro qualities such as mass, momentum, and temperature according to Eqs. (6) and (16), if the absolute difference of values between this and the last one is higher than the given small value, then go to step 2.
6. Save and output the values of temperature and velocity of the whole field.

Because the whole calculating process includes the collision and the flight of particles, it has a direct physical background.

3. Results and discussion

3.1. Validation of this model

The computing conditions are as follows: the calculation region is (8–16 mm) × (130–216.5 mm); the grid division is ((16–32) × (150–250)) * n, where n is decided by diffusion coefficient magnitude. The beginning values of LB evolution are given as $\vec{v} = 0$, $\rho = 0.02$ kg/m^3, $T = 300$ K. For convenience, dimensionless parameters are used in the calculation. The plasma is spraying in the air, the working gas is Ar and the diameter of the gun is 8 mm. The total effective viscosity of the plasma jet is calculated by Eq. (21) and the turbulent flow effect is decided by the sub-grid turbulence model. When the constant of the Smagorinsky model equals 0.008, the calculation results of the plasma jet along the jet centerline are compared with simulation and experimental results in paper [1], shown in Fig. 3. It can be seen from Fig. 3 that the simulation results by LBM and the sub-grid turbulence model agree with the experimental data given in paper [1]. The distribution trend of the velocity and the temperature distribution along the jet centerline are the same as that reported in paper [1].

3.2. Inlet velocity on jet

In Fig. 4, $T_0 = 14500$ K, $v_0^a = 400$ m/s, $v_0^b = 500$ m/s, $v_0^c = 600$ m/s, $v_0^d = 700$ m/s. Fig. 4 shows that when other conditions are the same, the flow characteristics of the plasma jet change with the jet-inlet velocity. It can be seen from Fig. 4 that there is no big variation of the isotherm distribution of flow field of the turbulent plasma jet compared with the change of the inlet velocity. When the inlet velocity of the plasma jet changes from 400 m/s to 700 m/s, the average extent of the velocity isotherm distribution is about 4 mm. And when the inlet velocity of the plasma jet changes from 500 m/s to 700 m/s, the average extent of the velocity isotherm distribution is about 3 mm. The temperature distribution of the plasma jet hardly changes though the variation extent of the inlet velocity attains several hundred meters per second. The calculation results accord with the experimental results in the published documents [17–19]. The experiments in the paper indicate that the jet

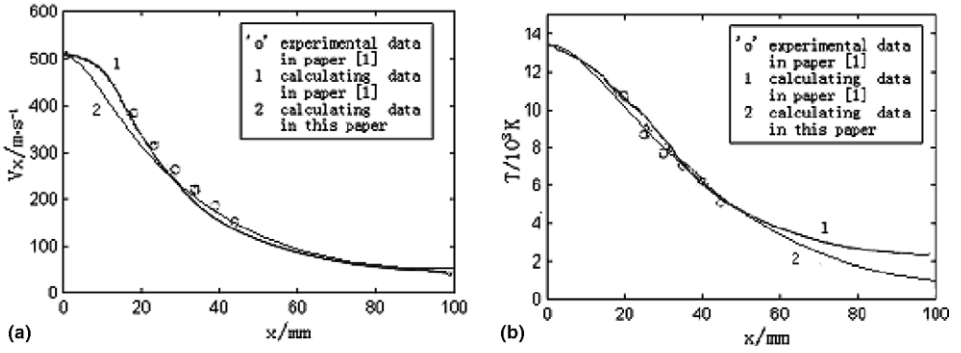

Fig. 3. Velocity and temperature distribution along the jet centerline.

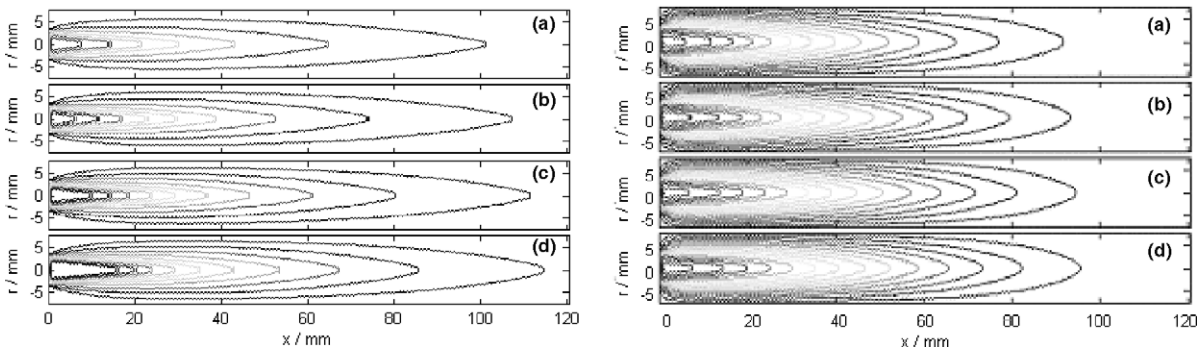

Fig. 4. (a) Axial velocity distribution with different exit velocities, 50 m/s for both the outer line and interval. (b) Temperature distribution with different exit velocities, 1000 K for both the outer line and interval.

field distribution and length of laminar plasma increase greatly with the increase of arc current and gas flow rate. But due to the effect of turbulence dissipation, the variety of jet field distribution and length of turbulent plasma are not obvious with change of the inlet velocity and temperature brought by the change of arc current and gas flow rate [17–19]. Fig. 4 also shows that the axial temperature gradient near the high temperature is higher than 200 K/mm and the velocity gradient attains 10 (m/s)/mm near a high-velocity zone, as in accordance with the experiments and simulations by the conventional method [17–20].

3.3. Inlet temperature on jet

Fig. 5 shows that along the centerline, the plasma jet temperature with higher inlet temperature declines faster under the same inlet velocity. Though at the same position the temperature with higher inlet temperature is still higher along the centerline, the length of the plasma jet is hardly affected by the inlet temperature. So enhancing the electric current can increase the inlet velocity and temperature, can accordingly increase the local temperature and the velocity distribution of the jet, but cannot obviously change the length of the turbulent plasma jet [17–19].

3.4. Flow field of velocity

Fig. 6 illustrates a flow field of the atmospheric plasma jet. In Fig. 6, $v_0 = 520$ m/s, $T_0 = 13340$ K. Fig. 6(a) presents the flow process of the jet as the LB evolution proceeds. Fig. 6(b) is the local enlarged flow field near the exit of the nozzle. The process of the plasma flow can be seen clearly according to Fig. 6(a) and (b) as the evolution proceeds. It can be seen from Fig. 6 that the plasma jet approaches a stable state after 2000 steps.

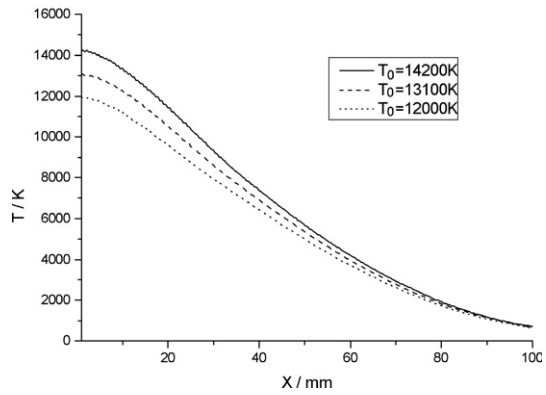

Fig. 5. Temperature distribution along centerline.

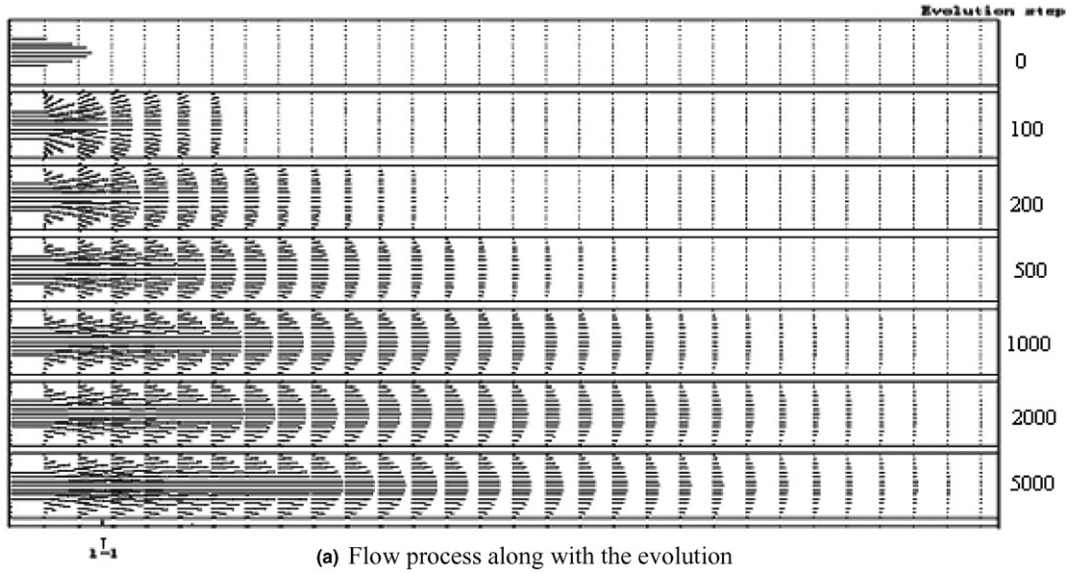

(a) Flow process along with the evolution

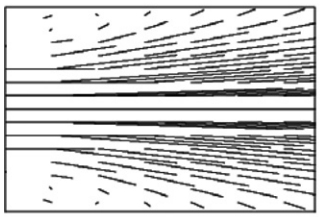

(b) Local enlarged flow field at exit 1-1

Fig. 6. Flow field of the atmospheric plasma jet.

Fig. 6(a) shows that the radial outspread and radial velocity of the jet are relatively obvious when the jet is just sprayed from the plasma nozzle. The radial velocity becomes small when the flow field attains a stable state. The closer the site along the section is to the jet axes, the smaller the radial velocity is. From the upper part of the jet to the lower part, the flow changes from a normal distribution to a parabolic distribution.

4. Conclusions

1. The LB plasma jet model is developed in this paper. The simulation by a current model is faster than that by the conventional methods because there is no iterative calculation in the simulation process. The method is feasible when v_0 is less than the local sound. The atmospheric pressure plasma jet meets the demand.
2. The plasma jet centerline temperature and the axial velocity obtained by the present model are comparable with those obtained by previous models and measurements. The LB plasma jet model, however, is found to be simpler and more intuitionistic than the traditional SIMPLE (or SIMPLEC) method. There is no need to solve the large equations set and to use stagger grids. Also, the bound is easy to be determined by LBM.
3. The statistic of LB equation depends on the time, so it is convenient for computing the non-steady fluid and also feasible for the steady fluid. In this paper, the fluid field can reach a steady state after 25 times of the number of axial grid.
4. Due to the effect of turbulence dissipation, the variety of jet field distribution and length of turbulent plasma are not obvious with increase of the inlet velocity and temperature brought by the enhancement of arc current and gas flow rate. Compared with the velocity at the inlet, the temperature at the inlet has a less influence on the characteristics of the plasma jet.

Acknowledgement

This research was funded by the National Natural Science Foundation of China through research Grants 50474053 and 50475134, respectively.

References

[1] E. Pfender, C.H. Chang, Plasma spray jets and plasma–particulate interaction: modeling and experiments, in: Proceeding of the 15th International Thermal Spray Conference, Nice, France, USA, vol. 1, 1998, pp. 315–325.
[2] Haiou Zhang, Rapid metal tooling technology, Electro. Mach. Mould 228 (2002) 6–8.
[3] Haiou Zhang, Guilan Wang, Nakga Takeo, Rapid hard tooling by plasma spraying for injection molding and sheet metal forming, Thin Solid Films 390 (2001) 7–12.
[4] He-Ping Li, Xi Chen, Three-dimensional simulation of a plasma jet with transverse particle and carrier gas injection, Thin Solid Films 390 (2001) 175–180.
[5] M. Boulos, P. Fauchais, E. PfenderThermal Plasmas, vol. 1, Plenum, New York, 1995.
[6] B. Jodoin, P. Proulx, Y. Mercadier, Numerical study of supersonic direct current plasma nozzle flow, AIAA J. 36 (1998) 578–584.
[7] Guilan Wang, Yanxiang Chen, Haiou Zhang, Effects of scanning path on the deposition process in rapid plasma spray tooling: modeling by homogenization theory, Thin Solid Films 435 (2003) 124–130.
[8] G. McNamara, G. Zanetti, Use of the Boltzmann equation to simulate lattice-gas automata, Phys. Rev. Lett. 61 (1988) 2332–2337.
[9] Y.H. Qian, Lattice BGK models for Navier–Stokes, Equat. Europhys. Lett. 17 (1992) 479–484.
[10] T. Chris, Hudong Chen, M. David, et al., Multi-speed thermal lattice Boltzmann method stabilization via equilibrium under-relaxation, Comput. Phys. Commun. 129 (2000) 207–226.
[11] Shiyi Chen, D. Doolen, Lattice Boltzmann method for fluid flows, Annu. Rev. Fluid Mech. 30 (1998) 329–364.
[12] S. Chapman, The mathematical theory of non uniform-gases, The Cambridge University Press, 1970.
[13] S. Hou, J. Stering, S. Chen, et al., A lattice Boltzmann subgrid model for high Reynolds number flows, Fields Inst. Comm. 6 (1996) 151–166.
[14] M. Lesieur, O. Metais, New trends in LES of turbulence, Annu. Rev. Fluid Mech. 28 (1996) 45–82.
[15] K. Akselvoll, P. Moin, Large-eddy simulation of turbulent confined coannular jets flows, J. Fluid Mech. 315 (1996) 387–397.
[16] C.M. Teixeira, Incorporating turbulence models into the lattice-Boltzmann method, Int. J. Mod. Phys. C 9 (1998) 1159–1175.
[17] Wenxia Pan, Generation of long, laminar plasma jets at atmospheric pressure and effects of flow turbulence, Plasma Chem. Plasma Process. 21 (2001) 23–30.
[18] Xian Meng, Wenxia Pan, Chengkang Wu, Temperature and velocity measurement of plasma jet, J. Eng. Thermophys. (China) 25 (2004) 490–492.
[19] Wenxia Pan, Xian Meng, Chengkang Wu, Length change of DC laminar-flow argon plasma jet, J. Eng. Thermophys. (China) 26 (2005) 677–679.
[20] E. Pfender, R. Spores, W. Chen, et al., A new look at the thermal and gas dynamic characteristics of a plasma jet, Int. J. Mater. Product Technol. 10 (1995) 548–565.